Research Article | Vol. 24, No. 22 | 31 Oct 2016 | OPTICS EXPRESS 25148

Optics EXPRESS

Stimulated Brillouin scattering enhancement in silicon inverse opal waveguides

M.J.A. SMITH,[1,*] C. WOLFF,[2] C. M. DE STERKE,[1] M. LAPINE,[2] B. T. KUHLMEY,[1] AND C.G. POULTON[2]

[1] *Centre for Ultrahigh bandwidth Devices for Optical Systems (CUDOS), Institute of Photonics and Optical Science (IPOS), School of Physics, The University of Sydney, NSW 2006, Australia*

[2] *Centre for Ultrahigh bandwidth Devices for Optical Systems (CUDOS), School of Mathematical and Physical Sciences, University of Technology Sydney, NSW 2007, Australia*

[*] *m.smith@physics.usyd.edu.au*

Abstract: Silicon is an ideal material for on-chip applications, however its poor acoustic properties limit its performance for important optoacoustic applications, particularly for stimulated Brillouin scattering (SBS). We theoretically show that silicon inverse opals exhibit a strongly improved acoustic performance that enhances the bulk SBS gain coefficient by more than two orders of magnitude. We also design a waveguide that incorporates silicon inverse opals and which has SBS gain values that are comparable with chalcogenide glass waveguides. This research opens new directions for opto-acoustic applications in on-chip material systems.

OCIS codes: (160.3918) Metamaterials; (290.5900) Scattering, stimulated Brillouin.

References and links

1. P. T. Rakich, C. Reinke, R. Camacho, P. Davids, and Z. Wang, "Giant enhancement of stimulated Brillouin scattering in the subwavelength limit," Phys. Rev. X **2**, 011008 (2012).
2. H. Shin, W. Qiu, R. Jarecki, J. A. Cox, R. H. Olsson III, A. Starbuck, Z. Wang, and P. T. Rakich, "Tailorable stimulated Brillouin scattering in nanoscale silicon waveguides," Nat. Commun. **4**, 1944 (2013).
3. C. Wolff, R. Soref, C. Poulton, and B. Eggleton, "Germanium as a material for stimulated Brillouin scattering in the mid-infrared," Opt. Express **22**, 30735–30747 (2014).
4. R. van Laer, B. Kuyken, D. van Thourhout, and R. Baets, "Interaction between light and highly confined hypersound in a silicon photonic nanowire," Nat. Photonics **9**, 199–203 (2015).
5. E. A. Kittlaus, H. Shin, and P. T. Rakich, "Large Brillouin amplification in silicon," Nat. Photonics **10**, 463 (2016).
6. R. van Laer, A. Bazin, B. Kuyken, R. Baets, and D. van Thourhout, "Net on-chip Brillouin gain based on suspended silicon nanowires," New J. Phys. **17**, 115005 (2015).
7. C. Wolff, R. van Laer, M. Steel, B. Eggleton, and C. Poulton, "Brillouin resonance broadening due to structural variations in nanoscale waveguides," New J. Phys. **18**, 025006 (2016).
8. C. J. Sarabalis, J. T. Hill, and A. H. Safavi-Naeini, "Guided acoustic and optical waves in silicon-on-insulator for Brillouin scattering and optomechanics," APL Photon. **1**, 071301 (2016).
9. B. J. Eggleton, C. G. Poulton, and R. Pant, "Inducing and harnessing stimulated Brillouin scattering in photonic integrated circuits," Adv. Opt. Photon. **5**, 536–587 (2013).
10. R. Pant, C. G. Poulton, D. Y. Choi, H. Mcfarlane, S. Hile, E. Li, L. Thevenaz, B. Luther-Davies, S. J. Madden, and B. J. Eggleton, "On-chip stimulated Brillouin scattering," Opt. Express **19**, 8285–8290 (2011).
11. C. Wolff, P. Gutsche, M. J. Steel, C. Poulton, and B. Eggleton, "Impact of nonlinear loss on stimulated Brillouin scattering," J. Opt. Soc. Am. B **32**, 1968–1978 (2015).
12. J. C. Tchahame, J.-C. Beugnot, K. P. Huy, V. Laude, A. Kudlinski, and T. Sylvestre, "Surface Brillouin scattering in photonic crystal fibers," Opt. Lett. **41**, 3269–3272 (2016).
13. O. Florez, P. F. Jarschel, Y. A. V. Espinel, C. M. B. Cordeiro, T. P. Mayer Alegre, G. S. Wiederhecker, and P. Dainese, "Brillouin scattering self-cancellation," Nat. Commun. **7**, 11759 (2016).
14. M. J. A. Smith, B. T. Kuhlmey, C. M. de Sterke, C. Wolff, M. Lapine, and C. G. Poulton, "Metamaterial control of stimulated Brillouin scattering," Opt. Lett. **41**, 2338–2341 (2016).
15. M. J. A. Smith, B. T. Kuhlmey, C. M. de Sterke, C. Wolff, M. Lapine, and C. G. Poulton, "Stimulated Brillouin scattering in metamaterials," J. Opt. Soc. Am. B **33**, 2162–2171 (2016)
16. K. S. Abedin, "Observation of strong stimulated Brillouin scattering in single-mode As_2Se_3 chalcogenide fiber," Opt. Express **13**, 10266–10271 (2005).
17. P. E. Powers, *Fundamentals of nonlinear optics* (CRC, 2011).
18. A. Kobyakov, M. Sauer, and D. Chowdhury, "Stimulated Brillouin scattering in optical fibers," Adv. Opt. Photon. **2**, 1–59 (2010).

#273954 http://dx.doi.org/10.1364/OE.24.025148
Journal © 2016 Received 17 Aug 2016; revised 17 Oct 2016; accepted 17 Oct 2016; published 19 Oct 2016

Optics EXPRESS

19. B. A. Auld, *Acoustic fields and waves in solids* (John Wiley & Sons, 1973).
20. D. Gaillot, T. Yamashita, and C. J. Summers, "Photonic band gaps in highly conformal inverse-opal based photonic crystals," Phys. Rev. B **72**, 205109 (2005).
21. A. Blanco, E. Chomski, S. Grabtchak, M. Ibisate, S. John, S. W. Leonard, C. Lopez, F. Meseguer, H. Miguez, J. P. Mondia, G. A. Ozin, O. Toader, H. M. van Driel, "Large-scale synthesis of a silicon photonic crystal with a complete three-dimensional bandgap near 1.5 micrometres," Nature **405**, 437–440 (2000).
22. B. G. Helme and P. J. King, "The phonon viscosity tensor of Si, Ge, GaAs, and InSb," Phys. Stat. Solidi A. **45**, K33–K37 (1978).
23. C. Wolff, M. J. Steel, B. J. Eggleton, and C. G. Poulton, "Stimulated Brillouin scattering in integrated photonic waveguides: Forces, scattering mechanisms, and coupled-mode analysis," Phys. Rev. A **92**, 013836 (2015).

1. Introduction

In recent years, considerable attention has been directed at enhancing stimulated Brillouin scattering (SBS) in silicon waveguides for on-chip applications [1–8]. However, the intrinsically poor properties of silicon has made photonic integration of SBS-based devices, such as Brillouin lasers and microwave signal processors, a fundamentally difficult task [9]. The poor performance of silicon in SBS applications can be attributed to a combination of high mechanical stiffness, low photoelasticity, and high acoustic losses, relative to other materials such as chalcogenide and silica glasses [10]. However, the existence of highly-refined fabrication facilities for silicon, together with the potential for integration with other photonic components, makes silicon an attractive platform for the cost-effective mass-production of SBS-based devices [9].

Existing work on the enhancement of SBS in silicon has primarily focused on waveguide designs that exploit radiation pressure (boundary motion) contributions to improve the electrostrictive response of the structure, treating the bulk properties of silicon as fixed. Here we propose a new method to enhance the SBS performance of silicon by using a metamaterial design based on silicon inverse opals. This involves structuring silicon with a lattice of interpenetrating spherical pores (see Fig. 1(a)). The principal outcome is that silicon inverse opals are less mechanically stiff than conventional silicon, which reduces the acoustic speed of sound in the material, enabling both light and sound to be confined within the same region. In addition, the reduction in the material quantity of silicon reduces acoustic losses, two-photon absorption (2PA), and free-carrier absorption (FCA) [11]. The porous-structuring of silicon thereby overcomes key fundamental constraints of silicon and gives it a clear advantage for SBS applications.

To the best of our knowledge, this is the first study on the bulk SBS properties of porous metamaterials, complementing recent work on the control of SBS in hollow-core silica fibres [12, 13] and recent theoretical work by the authors where metamaterials were shown to give enhancement and suppression of the bulk SBS [14, 15]. Here we report the extension of [14, 15] to interconnected pores and extend theoretical methods to evaluate all materials constants and wave propagation parameters present in the bulk SBS gain coefficient.

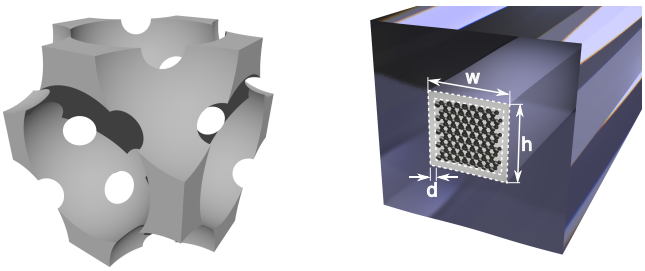

Fig. 1. (a) Fundamental unit cell for face-centred cubic (FCC) lattice of interpenetrating pores in silicon. (b) Waveguide design comprising silicon inverse opal core with silicon cladding (width d) embedded in fused silica substrate where w = 550 nm and h = 500 nm.

Optics EXPRESS

Having characterised the bulk properties of silicon inverse opals, we then numerically demonstrate the usefulness of the material with a waveguide design (see Fig. 1(b)). A fundamental issue with silicon waveguides is that whilst optical confinement is in principle straightforward, since the refractive index of silicon is high, acoustic mode confinement is difficult. The latter is due to the high speed of sound in silicon [1, 9] and the low speed of sound in common substrates such as fused silica glass [16]. The poor acoustic performance of silicon drives a poor acousto-optic overlap and subsequently weak SBS in a waveguide. Here we demonstrate that both a high refractive index and a low acoustic velocity can be achieved in bulk silicon inverse opals, which gives rise to much stronger acousto-optic overlap in silicon inverse opal waveguides. The improved acousto-optic overlap enhances the SBS gain in the waveguide to values comparable with uniform chalcogenide waveguides [3, 10] and germanium waveguides [3], and therefore has promising implications for silicon-based SBS devices.

2. Bulk SBS gain for a structured silicon

We first compute the SBS gain of a nanoscale-structured metamaterial comprising a face-centered cubic (FCC) lattice of interpenetrating pores in silicon ⟨100⟩ (see Fig. 1(a)). The period is chosen to ensure the metamaterial is both optically and acoustically subwavelength at an incident wavelength of $\lambda_1 = 1550\,\text{nm}$ and we assume negligible optical losses. The backwards SBS power gain coefficient for an incident optical plane wave propagating through a cubic or isotropic bulk material is [17, 18]

$$g_P = \frac{4\pi^2\gamma_{12}^2}{nc\lambda_1^2\rho V_\text{A}\Gamma_\text{B}}, \tag{1}$$

where $\gamma_{12} = p_{12}n^4$ is the electrostrictive stress induced by the incident optical field, p_{12} is the photoelastic constant (an element of the photoelastic tensor which applies for all plane wave polarisations), n is the refractive index, c is the speed of light in vacuum, ρ is the mass density of the medium, V_A is the longitudinal acoustic velocity, and Γ_B is the Brillouin line width.

We characterise the SBS properties of silicon inverse opals by calculating effective parameters for all optical, acoustic, and opto-acoustic terms present in (1) [14, 15]. Numerical results presented here are obtained using COMSOL 4.4 & 5.1. The photoelastic constant p_{12} is determined by mechanically perturbing the boundary of the unit cell and calculating the corresponding change in the effective inverse permittivity tensor. The deformed unit cell is obtained by solving the acoustic wave equation [19] under a static boundary loading with continuity conditions imposed at all mechanical interfaces. Unlike in previous work [14, 15], for a silicon inverse opal we must impose free-edge conditions $\sigma_{ij}\hat{n}_j\big|_{\partial I} = 0$ (solid-vacuum conditions) at all pore boundaries, where σ_{ij} denotes the stress tensor, and $\hat{n}_j$ is the normal vector to the internal boundary ∂I, in place of standard continuity conditions (solid-solid conditions). Whilst the calculation of the effective optical properties is unchanged from [14, 15], a subtle modification is required to calculate the acoustic parameters V_A and Γ_B: for these terms we solve the eigenvalue problem for the acoustic wave equation [19] with free edge conditions on ∂I, and acoustic Bloch conditions imposed only upon the remnants of the silicon background at the cell edge, since the pores do not form part of the acoustic domain.

With these modifications, we characterise the bulk properties of silicon inverse opals with pore volume filling fractions $f = 75\%$, 80%, and 85%. The range of filling fractions for an inverse opal is $74\% \lesssim f \lesssim 96\%$ where the bounds are the sphere-touching limit and the point where the two different inverse opal sites disconnect (i.e., when the tetrahedral and octahedral interstitial sites are no longer connected [20]). However, in practice this range is smaller because the material is not structurally stable at very high filling fractions. Here we impose an upper bound of $f = 85\%$ which is chosen to ensure that the interstitial site widths are of comparable size. This bound is close to $f = 88\%$ which is the greatest value achieved for micron-scale

Optics EXPRESS

Table 1. **Calculated bulk optical parameters, optoacoustic parameters, and SBS gain coefficient at $\lambda_1 = 1550$ nm.**[a]

f	a	n	p_{11}	p_{12}	p_{44}	g_P
75%	17.754	1.68	-0.10	0.18	-0.14	1.7×10^{-10}
80%	18.1818	1.53	-0.09	0.22	-0.15	3.9×10^{-10}
85%	18.6646	1.38	-0.05	0.23	-0.14	8.2×10^{-10}

[a] Here f is the porosity (pore volume filling fraction) for sphere radii a and lattice period $d = 50$ (both in units of [nm]), n the refractive index, p_{ij} the photoelastic tensor coefficients, and g_P the gain coefficient (units of [$W^{-1} \cdot m$]). Subscripts are represented in Voigt notation.

Table 2. **Calculated bulk acoustic parameters at $\lambda_1 = 1550$ nm**[b]

f	ρ	V_A	$\Omega_B/2\pi$	$\Gamma_B/2\pi$	C_{11}	C_{12}	C_{44}	η_{11}	η_{12}	η_{44}
75%	582.25	5210	11.3	21.3	15.81	7.96	6.8	0.42	0.34	0.042
80%	465.80	4591	9.1	9.6	9.82	5.55	4.12	0.18	0.14	0.018
85%	349.35	3985	7.1	3.8	5.55	3.57	2.15	0.07	0.06	0.007

[b] Here ρ denotes the mass density (in [$kg \cdot m^{-3}$]), V_A the longitudinal acoustic velocity (in [$m \cdot s^{-1}$]), $\Omega_B/(2\pi)$ the Brillouin frequency shift (in [GHz]), $\Gamma_B/(2\pi)$ the Brillouin linewidth (in [MHz]), C_{ij} are stiffness tensor coefficients (in [GPa]), and η_{ij} are phonon viscosity tensor coefficients (in [mPa · s]).

inverse opals [21].

Table 1 shows the calculated optical, opto-acoustic, and SBS parameters as a function of filling fraction. As expected, the refractive index of the metamaterial decreases with increasing porosity f. The photoelastic constant p_{12} increases with increasing f to values more than one order of magnitude greater than in pure silicon ($p_{12}^{Si} = 0.017$). Despite large enhancements in the photoelastic constant, which includes artificial photoelastic contributions [14, 15], the electrostrictive stress constant $\gamma_{12} = n^4 p_{12}$ decreases with increasing f because the drop in permittivity is much stronger. The gain coefficient increases with increasing filling fraction, due to positive contributions from all terms in (1) excluding γ_{12}. The increased gain can be understood with reference to the purely acoustic parameters in Table 2, which all decrease with increasing porosity. A reduced Brillouin linewidth has the biggest contribution to the gain enhancement, dramatically falling from $\Gamma_B^{Si}/(2\pi) = 320$ MHz to $\Gamma_B/(2\pi) = 3.8$ MHz at $f = 85\%$, and dominating improvements in all other terms. Such behaviour was previously observed for silica spheres in silicon [15] at high filling fractions. The improved optical and acoustic performance of porous silicon ultimately offsets the reduced γ_{12} to give a bulk SBS gain of $g_P = 8.2 \times 10^{-10}\,W^{-1}m$ at $f = 85\%$, more than two orders of magnitude above that of uniform silicon ($g_P^{Si} = 2.4 \times 10^{-12}\,W^{-1}m$).

We observe that bulk porous silicon with a porosity of $f \gtrsim 75\%$ has a sufficiently low stiffness to support confined acoustic modes, and for $f \lesssim 80\%$ it has a sufficiently high permittivity to support guided optical modes, inside a silica environment. This suggests that silicon inverse opal waveguides with $75\% \lesssim f \lesssim 80\%$ exhibit strong SBS. This is further investigated in Section 3. The values for p_{44} in Table 1 are obtained with the isotropic approximation $p_{44} = (p_{11} - p_{12})/2$, an approximation that is common in the optical, acoustic, and SBS literature. Also, we calculate η_{11} directly using SBS parameters [14], and set $\eta_{44} \approx \eta_{11}/10$, which is consistent with experimental data for semiconductors [22]. The remaining η_{12} element is then obtained using the isotropic approximation $\eta_{12} = \eta_{11} - 2\eta_{44}$. We find that these approximations for η_{12} and η_{44} do not affect the results substantially since all components of the viscosity tensor have a small magnitude. The use of an isotropic p_{44} slightly perturbs the gain values obtained for waveguides in Section 3, however, we anticipate that values calculated for the SBS gain in a waveguide are of the same order of magnitude.

Optics EXPRESS

3. SBS in a silicon waveguide

Having characterised the bulk properties of silicon inverse opals, we now investigate SBS in silicon inverse opal waveguides surrounded by a silica substrate, as would be required due to the need in a physical device to mechanically support the waveguide. We evaluate the SBS gain in a waveguide using the representation [23]

$$g_P^{\mathrm{wg}} = \left(\frac{4\pi c}{\lambda_1 |P| U_{\mathrm{A}}}\right) |\xi|^2 Q_{\mathrm{A}}, \tag{2}$$

where P denotes the energy flux for the optical mode, U_{A} is the energy density of the acoustic mode, ξ is the opto-acoustic overlap integral, and Q_{A} is the acoustic quality factor of the waveguide, and the brackets contain normalisation factors.

In principle, a simple design comprising a rod of porous silicon embedded in silica confines both sound and light and can therefore support SBS. However, the low dielectric contrast and relatively low stiffness of silicon inverse opals means that the SBS-gain of such structures is low; the optical and acoustic modes extend well into the substrate, resulting in poor opto-acoustic overlap. The waveguide we propose is shown in Fig. 1(b), and comprises a silicon inverse opal core surrounded by a silicon cladding layer that is suspended in fused silica. The thickness of the silicon shell layer plays an important role in the predicted SBS gain, and here we investigate optimal layer widths surrounding an inverse opal core. Introducing an additional layer of unstructured silicon around a core of porous silicon (see Fig. 1(b)) improves both the optical and the acoustic confinement through two distinct mechanisms. Optical confinement is improved by the high permittivity of the cladding, as the silicon walls bear some similarity to a slot waveguide. Acoustic confinement is improved by the high stiffness of the silicon shell which reduces the tails of the acoustic mode in the silica cladding. This reduction of the optical and acoustic mode areas enhances the overall SBS-gain of our waveguide to levels competitive with experimentally demonstrated SBS platforms.

Figure 2 shows results from a parameter study for our waveguide design, which has a total width $w = 550$ nm and height $h = 500$ nm, and in which we vary the porosity f of the porous core and the thickness d of the unstructured silicon. The effective material parameters from Section 2 were used for the waveguide core domain, and were interpolated where necessary. Bulk values for silicon and fused silica are given in [14]. We evaluate the acousto-optic overlap as in [23], with $Q_{\mathrm{A}} = \Omega_{\mathrm{B}}^{\mathrm{wg}}/\Gamma_{\mathrm{B}}^{\mathrm{wg}}$, where the line width is given by the integral of the dynamic viscosity tensor [14]. Figure 2(a) shows the gain coefficient g_P^{wg} versus filling fraction f and silicon shell thickness d. A maximum of $g_P^{\mathrm{wg}} = 193\,\mathrm{W^{-1}m^{-1}}$ occurs at ($f = 80.7\%, d = 55$ nm) which is comparable with values for chalcogenide ($\approx 300\,\mathrm{W^{-1}m^{-1}}$ [3, 10]), partially suspended silicon ($\approx 350\,\mathrm{W^{-1}m^{-1}}$ [4]), and germanium ($\approx 488\,\mathrm{W^{-1}m^{-1}}$ [3]) waveguides. The gain is low for small f and large shell thickness due to poor acousto-optic overlap. In Fig. 2(b) we show $\log_{10}(Q_{\mathrm{A}})$, where the low Q_{A} region for high f is due to acoustic cutoff in the waveguide. Figure 2(c), showing the Stokes shift $\Omega_{\mathrm{B}}^{\mathrm{wg}}/(2\pi)$ [GHz] for the waveguide, indicates that the large variations in Q_{A} are caused by the acoustic loss in the waveguide. The Stokes shift is seen to vary smoothly over the parameter space and, since, $V_{\mathrm{A}}^{\mathrm{wg}} \propto \Omega_{\mathrm{B}}^{\mathrm{wg}}$, shows that the acoustic velocity changes by as much as 33%. In Fig. 2d we present the norm of the transverse electric field $\sqrt{|E_{\mathrm{x}}|^2 + |E_{\mathrm{y}}|^2}$ and the norm of the transverse acoustic field $\sqrt{|u_{\mathrm{x}}|^2 + |u_{\mathrm{y}}|^2}$ at ($f = 80\%, d = 50$ nm), which is close to the values for the optimal gain. Here $\mathbf{u}$ is the acoustic displacement vector and $\mathbf{E}$ denotes the electric field. These mode profiles clearly demonstrate that the optical and acoustic fields for SBS in our silicon waveguide are strongly confined.

The electric field discontinuities at the silicon-silica and the silicon-metamaterial boundaries are small in our waveguide and so radiation pressure contributions to the SBS gain are negligible.

Optics EXPRESS

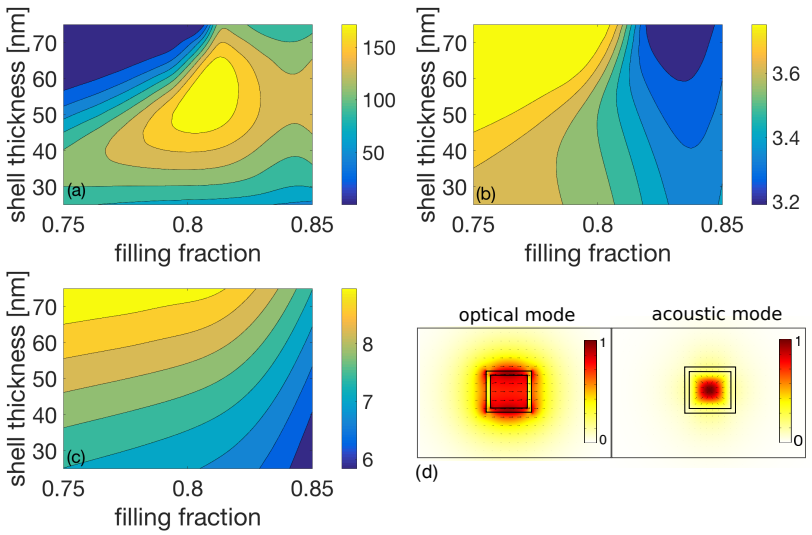

Fig. 2. (a) SBS power gain coefficient $g_P^{\mathrm{wg}}\left[\mathrm{W}^{-1}\mathrm{m}^{-1}\right]$ versus porosity f in the core and silicon shell thickness d; (b) $\log_{10}(Q_{\mathrm{A}})$ where Q_{A} is acoustic quality factor; (c) Stokes shift $\Omega_{\mathrm{B}}^{\mathrm{wg}}/(2\pi)$ [GHz]; and (d) Optical and acoustic modes at ($f = 80\%, d = 50$ nm) where the colorscales (arb. units) refer to $\sqrt{|E_x|^2 + |E_y|^2}$ and $\sqrt{|u_x|^2 + |u_y|^2}$, respectively.

4. Discussion and conclusions

We have theoretically demonstrated that the bulk SBS gain coefficient of silicon can be enhanced by two orders of magnitude using a metamaterial design based on silicon inverse opals. This enhancement is due to the larger compressibility of the inverse opal, which lowers the acoustic velocity, and the reduced Brillouin linewidth. We also design a waveguide based on this material that demonstrates gain values comparable to chalcogenide waveguides, possessing the added advantage of lower 2PA and lower FCA than in unstructured silicon (note that the large internal surface in the porous structure will reduce carrier lifetime and therefore further diminish the impact of FCA). Further work includes developing a full numerical procedure for the shear terms of the effective photoelastic and phonon viscosity tensors, which is difficult to implement in standard FEM solvers, and studying forward SBS in silicon inverse opals, which is promising given the strong experimental performance of forward SBS in fully and partially etched silicon waveguides ($\approx 2000 - 10000\,\mathrm{W}^{-1}\,\mathrm{m}^{-1}$) [2, 4–6].

From a practical perspective, fabricating our metamaterial will require precision, since, for example, variations in the pore radii and positions lead to attenuation through Rayleigh scattering. Similarly, effects such as inhomogeneous linewidth broadening [7] and squeeze-film damping are important considerations for the waveguide design. However, there have been successful attempts at creating high-quality inverse opals in silicon [21] and such techniques may be refined to create the types of waveguide structures presented here.

Funding

Australian Research Council (ARC) (CE110001018, DP150103611).